



Full length article

Reactive modeling of Mo₃Si oxidation and resulting silica morphology

Chamila C. Dharmawardhana^a, Jihan Zhou^b, Matthew Taylor^c, Jianwei Miao^b,
John H. Perepezko^c, Hendrik Heinz^{a,*}

^a Department of Chemical and Biological Engineering, University of Colorado Boulder, 596 UCB Boulder, CO 80309, USA

^b Department of Physics & Astronomy and California Nano Systems Institute, University of California, Los Angeles, CA 90095, USA

^c Department of Materials Science and Engineering, University of Wisconsin-Madison, Madison, WI 53706, USA



ARTICLE INFO

Article History:

Received 13 October 2019

Revised 7 January 2020

Accepted 23 January 2020

Available online 26 January 2020

Keywords:

Mo alloy

A15 phase

Corrosion

Reactive molecular dynamics

Silica

ABSTRACT

Oxidation and corrosion have a significant economic footprint. Mo-based alloys are a strong candidate for structural materials with oxidation resistance at high temperatures. However, understanding of the mechanisms remains limited as experimental techniques do not reach atomic-scale resolution. We examined the mechanism of oxidation of Mo₃Si (A15 phase) in Mo–Si–B alloys, the emergence of a superficial silica scale, and explain available experimental data up to the large nanometer scale using chemically detailed reactive simulations. We introduce new simulation protocols for layer-by-layer oxidation and simple force fields for the reactants, intermediates, and products. Growth of thin superficial silica layers as a function of temperature and oxidation rate on the (001) surface involves the formation of silica clusters, rings, and chains with pore sizes of 0 to 2 nm. An increase in temperature from 800 to 1000 °C slightly decreased the pore size and lead to less accumulation of Mo oxides at the interface, consistent with observations by electron tomography and energy dispersive X-ray spectroscopy (EDS). The elimination of gaseous MoO_x is essential to form open channels and much larger pores up to 100 nm size as observed by 3D tomography, in-situ transmission electron microscopy (TEM) and scanning electron microscopy (SEM) as the oxide phase grows. According to the simulation, these large pores would otherwise be closed. The rate of oxidation, represented by successive oxidation of layers of variable thickness per unit time, influences the structure and cohesion of silica layers. High rates of oxidation can destabilize and break apart the silica layer, supported by a very wide pore size distribution in electron tomography. Limitations of the simulations in time scale currently restrict the analysis to few-layer oxidation. Within these bounds, the proposed simulation protocols can provide insight into the oxidation of (hkl) surfaces, grain boundaries, and various alloys compositions up to the 100 nm scale in atomic-level detail.

© 2020 Acta Materialia Inc. Published by Elsevier Ltd. All rights reserved.

1. Introduction

Oxidation and corrosion are a challenge that consumes about 3.4% of the global gross domestic product [1]. Much of this cost distributes across industry sectors such as transportation and building infrastructure, defense, and aerospace, consuming valuable natural resources. For example, jet engines and power turbines are exposed to some of the hottest environments that materials have to bear [2]. The operational demands of such devices expound the physical limits of present-day Ni-based super alloys and limit the feasible lifetimes [3]. Customized cooling systems allow for increased temperature operation of the engines at the expense of reduced efficiency, however, they also pose a heavy burden on the energy requirements and increase environmental pollution [4].

Alternative candidate alloys require a high melting temperature (T_m), high tensile strength, sufficient ductility, fatigue resistance, and above all oxidation resistance. Example metal components are Mo and Nb, and Mo–Si–B alloys have become a prime candidate for meeting these goals as reported in several studies [2,4,5]. One of the primary advantages of Mo–Si–B alloys over competing Nb-based alloys is a higher melting temperature and expected superior oxidation resistance. Compared to Nb-oxides, a protective borosilicate layer formed on Mo–Si–B alloys is believed to be the main reason for this higher, yet not adequately studied oxidation resistance. Nevertheless, studies on oxidation resistance have been mainly conducted at the microscale [6]. A broader adoption of Mo–Si–B alloys for high temperature applications hinges on understanding the oxidation characteristics.

Therefore, it is essential to understand the mechanism of silicate formation across the various stages of oxidation from the atomic scale to the microscale. Among various molybdenum silicides, Mo₃Si (an A15 phase) is the most Mo-rich phase and expected to oxidize

* Corresponding author.

E-mail address: hendrik.heinz@colorado.edu (H. Heinz).

faster [5]. In this study, we employ to-date unused molecular dynamics (MD) methods with a novel reactive force field to analyze the surface oxidation mechanisms of Mo₃Si from the atomic scale to the large nanometer scale at realistic temperatures. No prior simulations have been reported at this scale due to lack of methods and suitable potentials, and current experimental techniques do not reach a resolution higher than few nanometers. The reactive force field is based on the Interface force field (IFF) [7], which was augmented to describe the alloy, silica, and MoO₃ by nonbonded-only interactions that allow unbiased changes in silica morphology upon oxidation of the alloy phase [8–10].

A high percentage of the Mo phase in Mo–Si–B alloys is important to provide ductility in targeted mechanical applications, however, the Mo phase also reduces the oxidation resistance due to volatile MoO₃ formation at high temperature. Therefore, all aspects of oxidation must be carefully studied in order to reach a balance between good mechanical properties and minimal corrosion. Mo–Si–B alloys begin to oxidize at a temperature of ~500 °C with a rapid weight gain due to the formation of oxide. Between 500 and 650 °C, the alloy experiences a linear weight loss due to initial MoO₃ sublimation and borosilica formation [6,11]. The next stage of 650–750 °C involves most rapid oxidation accompanied by sublimation of volatile MoO₃ gas and migration of initially formed MoO₂ solid across the surface. Interestingly, pure MoO₃ melts at 795 °C and boils at 1155 °C [12] while Floquet et al. observed in an x-ray study that pure Mo forms MoO₃ and evaporates rapidly above ~500 °C leaving small voids [13]. Likely, the exothermic heat of formation leads to a higher local temperature at the surface than the average temperature, inducing sublimation of MoO₃. Violent MoO₃ evaporation in this intermediate temperature range initiates what has been called the “pesteing process” [14]. The pesteing process in molybdenum silicides is the accelerated oxidation that results in disintegration of the compound to a lump of powder [4,15]. It is then likely that the viscous oxides of silicon and molybdenum do not form a continuous layer, which would slow down the oxidation. Above 800 °C, however, a continuous and less viscous oxide layer forms that slows down the oxidation process and the mass loss due to forced evaporation of MoO₃ [6,16,17]. Pure silica versus borosilica hereby affects the retardation of oxidation differently. Some studies with Al impurities introduced into the A15 phase (Mo₃Si) also reported a reduced mass loss [18,19]. These complex oxidation processes are not yet well understood and more in-depth knowledge of the mechanisms, especially at high temperature, is important. The silica morphology, and especially porosity, are important factors that control and inhibit further oxidation of the A15 phase as the accessibility of the alloy surface by oxygen is reduced.

While it is not feasible to answer all open questions in a single study, simulations can effectively complement experimental imaging and dynamic *in-situ* monitoring of the oxidation reactions. However, to-date, modeling of an oxidation or corrosion process at a practical scale has been difficult even for simplest materials. *Ab initio* techniques are prohibitively expensive for large scale simulations at realistic temperatures such as the present study, even with the simplest energy functionals and basis sets [20,21]. Surface energies of metals also deviate up to 50% from experimental values even with advanced density functionals [22,23]. In contrast, recent force fields such as IFF reproduce surface and interfacial properties with less than 10% deviation from experiment [7,10] and have shown quantitative predictions in modeling crystal growth [24,25], surface catalysis [26], and induced charges [27]. Therefore, we choose molecular dynamics techniques with force fields tailored for reactive surface simulations, and a new method to probe layer-by-layer oxidation of the alloy. Using new models for the alloy and the key oxide phases, this study provides new insight into the dynamics and mechanisms of the oxidation reaction (Fig. 1a), the role of MoO₃ evaporation, and resulting silica morphologies for different temperatures and reaction rates. We

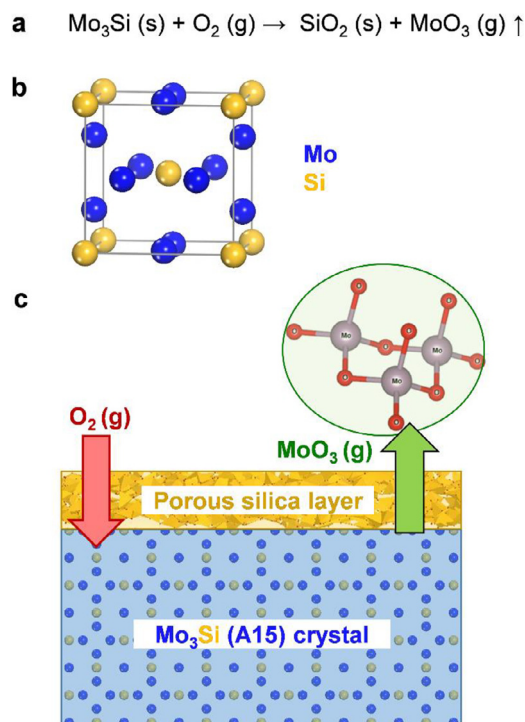


Fig. 1. The oxidation reaction of Mo₃Si, the structure of the unit cell, and a schematic of the reaction in an atomistic model. (a) The reaction on the surface of Mo₃Si above 800 °C leads to an amorphous layer of silica and forced evaporation of MoO₃ gas. (b) A model of the unit cell of Mo₃Si, shown for an ideal geometry of the A15 intermetallic phase (β -W). Si atoms form a bcc superlattice and the Mo atoms occupy positions on the faces. X-ray data for Mo₃Si show some deviations from the ideal A15 structure (ref. [32]). (c) The oxidation reaction leads to formation of a superficial porous silica layer. Incoming oxygen molecules diffuse through this layer and react with the alloy surface, generating MoO₃ gas and growing the porous silicon dioxide layer. The preferred structure of gaseous MoO₃ is a trimeric cluster (see inset and ref. [33]). (For interpretation of the references to colour in this figure legend, the reader is referred to the web version of this article.)

employ models of the common (001) surface of Mo₃Si (Fig. 1b) and simulate the oxidation reaction on the 10–100 nm scale (Fig. 1c) in comparison to TEM data [28], electron tomography [29,30] and EDX measurements [31].

2. Methods

In the following, model building, the simulation protocol for the oxidation reaction, the analysis of mechanisms and product structure including pore size, and the force field parameterization are described.

2.1. Model building

Models of Mo₃Si were built using the cubic Mo₃Si crystal structure according to data from X-ray diffraction [32]. The unit cell contains eight atoms (six Mo and two Si atoms) (Fig. 1b). Si atoms are located at the corners and at the center of a BCC superlattice while two Mo atoms reside on each face representing mutually orthogonal planes. We employed $10 \times 10 \times 10 \text{ nm}^3$ supercells for most simulations as well as $100 \times 100 \times 100 \text{ nm}^3$ supercells for large-scale simulations, containing approximately 64 million atoms, to explore the size-dependence of silica morphology.

2.2. Protocol for reactive simulations

We employed a new protocol of layer-by-layer oxidation of the intermetallic compound and relaxation of the products after every

reaction cycle by molecular dynamics simulation (Fig. 2a). The simulation of the reaction started with a model of crystalline Mo₃Si. Upon identification of the topmost atomic layer on the (001) surface of Mo₃Si, adjustments in the composition from reactants to products were made, including the correct stoichiometry of the reaction and relaxation of the oxide products by molecular dynamics simulation. Details of the reaction mechanism on the scale of individual bonds, including O₂ dissociation and elementary steps of forming SiO₂ and MoO_x were disregarded in this first study because current understanding is rather limited and the computational implementation would be difficult. The (001) surface was chosen since it has the lowest surface energy of ~2.5 J/m² in comparison to (110) and (111) facets according to DFT calculations (Table S1 and Section S1 in the Supplementary Information). The (001) surface likely covers a dominant portion of the Mo₃Si surface, and the computed surface energy is close to a stoichiometric average of experimental surface energies for Mo and Si (~2.5 J/m²) [34].

In more detail, (1) first an atomic layer on the (001) surface of a given thickness was converted from the metallic state to the oxide state by addition of O atoms above the surface (Fig. 2a) to match the SiO₂ stoichiometry, and Mo atoms were replaced with MoO₃ molecules (one Mo replaced with a monomer unit of MoO₃). A typical layer thickness per reaction cycle was 0.25 nm, and the layer thickness was varied to model different reaction rates (Fig. 2b). (2) Atomic charges and atom types (force field types) for Si and Mo in the reaction layer were changed from those used in the alloy to those used in the oxides to represent the new chemical environment. The new atom types and charges describe Si and O in silica (SiO₂) with an approximate nonbonded potential that allows structural changes. We also employed one potential type for MoO₃, which was represented as a single coarse grain bead for simplicity and to enable experimental-scale simulations (Table 1). (3) After the reaction of the chosen atomic layer, molecular dynamics simulation in the NVT ensemble was carried out for 200 ps to relax the updated silica

Table 1
Force field parameters for silica, bulk Mo₃Si alloy, and MoO₃ gas.

atom/unit	charge (e)	12–6 LJ (CVFF, CHARMM, AMBER)	
		σ_{ii} (Å)	ϵ_{ii} (kcal/mol) ^a
Si (silica)	+2.4 ^b	1.80	0.300
O (silica)	-1.2	3.47	0.027
Mo (metal)	0.0	2.99	5.0
Si (metal)	0.0	4.55	3.0
MoO ₃ (gas) ^c	0.0	4.49	0.3 ^d

^a The unit kcal/mol is routinely used in many simulation programs and therefore given here (LAMMPS, NAMD, Forcite). Equivalent values in kJ/mol are 1.26, 0.113, 20.9, 12.6, and 1.26 from top to bottom, respectively.

^b Partially oxidized Si atoms at the alloy-SiO₂ interface with SiO stoichiometry were assigned a + 1.2e charge.

^c Represented as a coarse-grain bead.

^d Higher epsilon values up to 1.0 kcal/mol were tested at $T < 900$ °C, then leading to larger pore size.

morphology and allow the MoO₃ gas to evaporate at the selected temperature (800, 900 or 1000 °C). The time step was 1 fs and the pairwise summation of van-der-Waals interactions employed a cutoff of 10 Å (shorter than typical 12 Å to increase speed). Coulomb interactions were computed using the PPPM method with a high accuracy of 10⁻⁴. (4) Then, the next atomic layer was oxidized and the system relaxed by molecular dynamics simulation again. The reaction sequence was repeated until a certain portion of the model slab of Mo₃Si was oxidized. After the reaction cycles were completed, the model system was cooled down from the reaction temperature to room temperature over a period of 1 ns by further MD simulation to stabilize the silica layer formed on top of the Mo₃Si phase and carry out the analysis.

All atoms and beads of the oxide phases had full 3D mobility, however, the positions of the atoms in the Mo₃Si phase were fixed to help preserve the crystal structure of the alloy and decrease the computational cost. The high melting point of the bulk alloy phase of 2025 °C [35] supports the neglect of the dynamics at 800 to 1000 °C via fixed atomic positions of the alloy. The temperatures in the simulation were chosen as 800, 900 and 1000 °C to represent typical laboratory conditions and facilitate comparisons with measurements [31]. Thermal expansion of Mo₃Si was taken into account by increasing the lattice parameter according to the thermal expansion coefficient from experiment [36].

2.3. Inclusion versus neglect of MoO₃ evaporation

In the first set of simulations, MoO₃ evaporation was disregarded by simply deleting Mo atoms from the intermetallic phase during the reaction and restricting oxidation to Si atoms only. This setup helped explore the limit of infinitely slow molybdenum trioxide evaporation and development of a silica scale of the highest possible density, which is challenging to explore in experiment. All other simulations incorporated the formation of silica, MoO₃, and evaporation of MoO₃ gas, which exits from the surface and changes the silica morphology depending on temperature and oxidation rate.

2.4. Broader utility of the simulation method

The stepwise (layer-by-layer) oxidation protocol can be used to simulate the oxidation reaction of any alloys using molecular dynamics simulation (Fig. 2). The method mimics the typically slow oxidation process one atomic layer at a time. The use of simple potential functions can keep the computational cost comparatively low and enable the analysis of sample models up to micrometer-size in one, two, or possibly all three dimensions. The oxidation rates in the simulation still remain faster than in experiment (several cm per second). However, slower oxidation rates could be investigated in follow-on

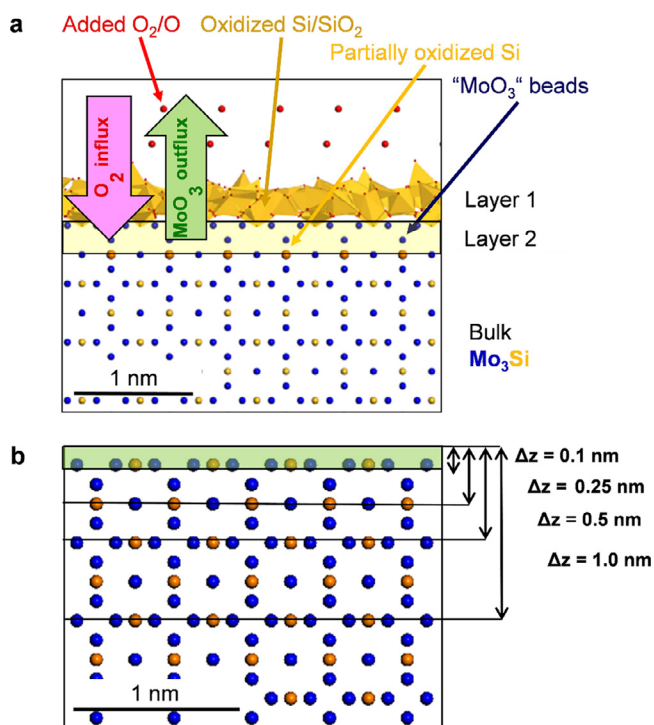


Fig. 2. Simulation protocol for the oxidation reaction of Mo₃Si and formation of a superficial silica layer. (a) Sequential oxidation of the Mo₃Si alloy phase one monolayer at a time on the thermodynamically stable (001) facet. (b) The relative rate of oxidation was varied using various increments per reaction cycle of $\Delta z = 0.1, 0.25, 0.5$ and 1.0 nm.

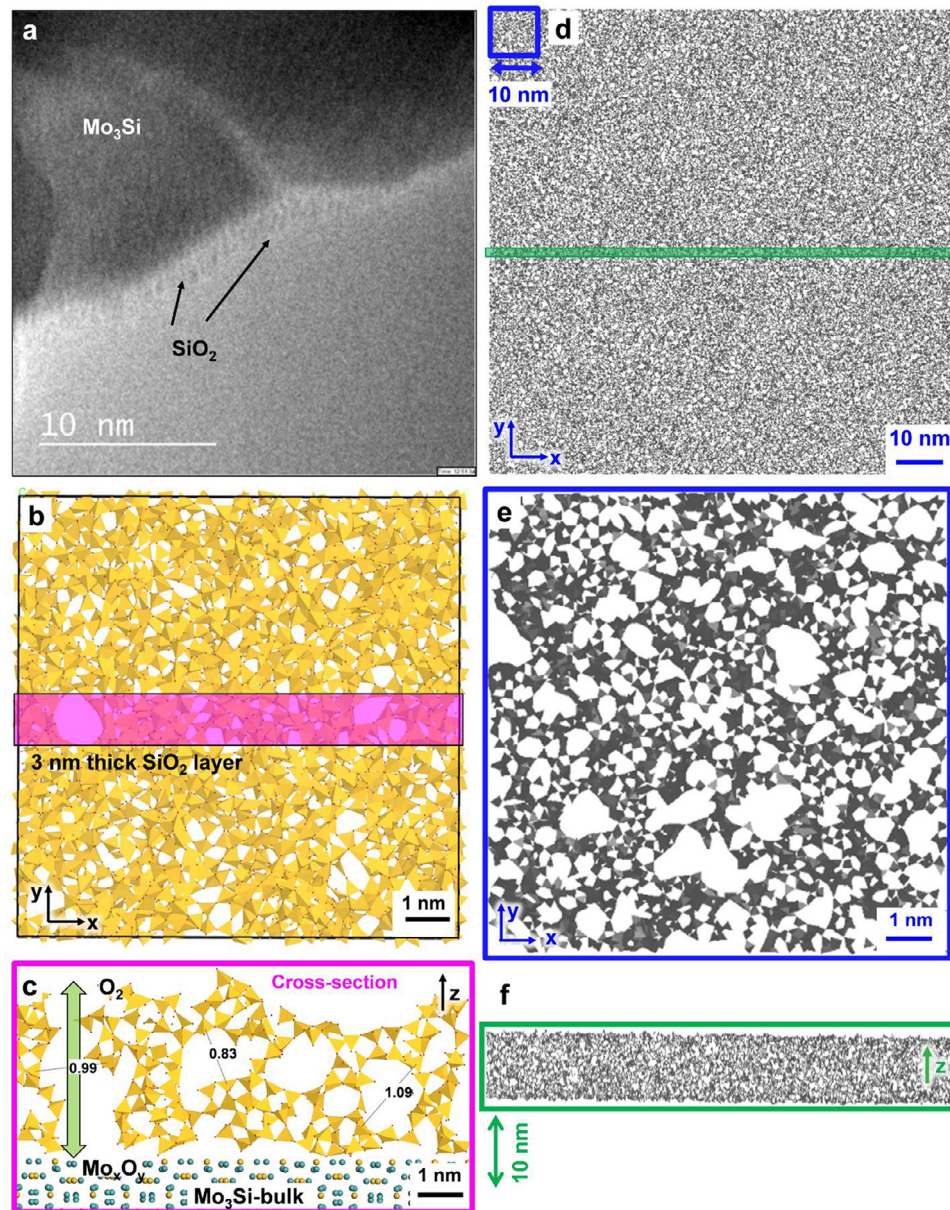


Fig. 3. Silica morphology after Mo_3Si oxidation according to TEM and reactive molecular dynamics simulation, neglecting MoO_3 evaporation. (a) *In-situ* TEM image of an oxidized Mo_3Si sample with 2 to 3 nm thickness of the silica layer (24 mins, 800 °C, from ref. [28]). (b) Top view onto the morphology of a 3 nm thick silica layer from reactive simulations at 800 °C ($10 \times 10 \text{ nm}^2$ model in the x-y plane). A 1 nm wide slab is highlighted (pink), and silica tetrahedra are shown in yellow. (c) Side view of the highlighted slab in (b) in the y-z plane. A ~1 nm wide channel and the pore structure can be seen. (d) Top view onto the morphology of a 10 nm thick silica layer from reactive simulations using a larger model of $100 \times 100 \text{ nm}^2$ size with 64 million atoms in the x-y plane. Simple removal of Mo atoms without MoO_3 evaporation was assumed. A small area (blue) and 1 nm wide slab (green) are highlighted. (e) Magnified top view onto the $10 \times 10 \text{ nm}^2$ highlighted area in blue in (d). A similar pore structure as in the 2–3 nm thick layer in (b) can be seen, including small continuous regions and pores between 0 and 2 nm in size. (f) Side view of the 10 nm thick highlighted silica slab (green) in (d) in the y-z plane. The porosity is retained, however, open channels are rare to find. (For interpretation of the references to colour in this figure legend, the reader is referred to the web version of this article.)

work, for example, by oxidizing only a fraction of an atomic layer per nanosecond, starting with islands and progression in patterns across the surface.

2.5. Specific simulation settings

The Mo_3Si model slabs of $10 \times 10 \times 10 \text{ nm}^3$ and $100 \times 100 \times 100 \text{ nm}^3$ size had 3D periodicity, including a thick added vacuum slab atop the (001) surface in z direction. This setup effectively leads to periodicity in x and y directions and an exposed (001) surface (Figs. 2 and 3). For each layer oxidized, Mo atoms were reassigned coarse-grained, non-bonded parameters and zero net charge to represent MoO_3 . The oxidized Si atoms were reassigned the potential type and charge of silica, and an appropriate number of O atoms was added above the silica

layer (Fig. 2a). The O atoms then migrated through the silica layer to react with the newly released Si atoms at the interface and integrated into the existing silica layer (see Movie S1). The topmost layer of Si atoms at the alloy/silica interface was partially oxidized (Fig. 2a) with a charge of +1.2e, and O atoms were added in a 1:1 ratio with a charge of -1.2e on top of the partially oxidized silica layer to compensate the charge. The partially oxidized Si atoms also remained part of the bulk alloy with fixed atomic positions and ensured cohesion at the alloy-silica interface. The silica layer was thus affected by the influx of O atoms from above and by the MoO_3 beads flowing outwards from the interface (Fig. 2b). The two fluxes of O atoms and MoO_3 are directly dependent upon the thickness (Δz) of the oxidized layer in each simulation cycle. The conversion of Mo to MoO_3 also imposes some restraints on the reactive simulation. Assuming layer-by-layer oxidation cycles, the layer thickness (Δz) considered for each

cycle of the reaction needs to be a multiple of the number of atomic layers to allow adhesion of the silica layer to the alloy surface at all temperatures (Fig. 2b). Therefore, we tested oxidation rates that correspond to intervals of $\Delta z = 0.1, 0.25, 0.5$ and 1 nm for each oxidation step. A larger interval (higher Δz) hereby represents a higher relative oxidation rate. The relation of these assumptions to experimental conditions and analysis of their effects help in understanding the oxidation process (see Section 3.3).

2.6. Analysis of silica porous structure by stochastic ray tracing

The silica layer formed upon Mo_3Si oxidation is a network of pores of irregular shape [37]. Characterization of a porous network is a difficult task, especially for irregular shapes and sizes of the pores in the distribution [31]. Several methods are available to characterize the porosity of the sample when the atomic coordinates are known, and most of these methods work specifically for 3D periodic systems [38–40]. One method that has been successfully used to analyze porous zeolitic crystalline phases [38,41] was extended here to characterize the porosity of surface silica for the first time. The estimation of the pore distribution is based on a Monte Carlo ray tracing algorithm introduced by Willems *et al.* [38] and implemented in the Zeo+ program. The algorithm places a random spherical probe of predefined diameter (0.1 Å) within the porous silica layer. The probe is then moved until it intersects with silica units which define a “ray” of certain length. The statistics of ray lengths are representative of the pore size distribution [42]. We utilized this method to quantify the porosity of the silica layers.

2.7. Force field parameters for reactive simulations

We chose a widely used harmonic energy expression compatible with multiple force fields such as the Interface force field (IFF), CHARMM, CVFF, AMBER, and OPLS-AA to allow reliable simulations of inorganic compounds and interfaces with water and organic compounds [7,43]. The simulation of mixed oxides, phase transitions, and morphological changes can be easier accomplished by using only non-bonded energy terms since a bonded network with terms for bond stretching and angle bending would constrain the morphology and phase composition [44,45]. The simplified expression for the potential energy E_{pot} consisted of a term for Coulomb interactions and a term for a 12–6 Lennard-Jones potential:

$$E_{\text{pot}} = \frac{1}{4\pi\epsilon_0} \sum_{ij, \text{nonbonded}} \frac{q_i q_j}{r_{ij}} + \sum_{ij, \text{nonbonded}} \epsilon_{ij} \left[\left(\frac{\sigma_{ij}}{r_{ij}} \right)^{12} - 2 \left(\frac{\sigma_{ij}}{r_{ij}} \right)^6 \right] \quad (1)$$

Bonded terms such as bond, angle, torsion, out-of-plane, or Urey–Bradley potentials were zero without loss of generality [43].

We utilized six different atom types, including Mo and Si in solid Mo_3Si , Si and O in SiO_2 , and coarse-grain beads of MoO_3 , as well as a type of partially oxidized Si atoms on the alloy surface with half the atomic charge of Si in SiO_2 . The metal atoms Mo and Si in the A15 phase were of zero atomic charge and the Lennard-Jones parameters approximately reproduce the density and the surface energy [10]. No dedicated validation of the LJ parameters for Mo and Si was carried out as the atoms in the Mo_3Si lattice remained fixed.

A set of nonbonded parameters for silica was derived from bonded parameters in IFF [9]. The nonbonded parameters consist of atomic charges q_i and Lennard-Jones parameters σ and ϵ for Si and O atoms (Table 1). The polarity of Si-O bonds in silica corresponds to atomic charges of $+1.0e$ to $+1.1e$ for Si and $-0.5e$ to $-0.55e$ for O [9,46]. In comparison to a formal charge of $+4e$, ionic bonding contributes approximately 25% and covalent bonding 75%. In the nonbonded model, atomic charges were increased to account for the total cohesion due to internal dipoles and due to localized chemical bonding. Since ionic contributions to bonding scale with the square of the atomic charge, an increase of the Si charge near $+2.0e$ approximately increases the ionic

contribution to the cohesive energy from 25% to 100%, whereas a formal charge of $+4e$ would strongly overestimate the total bonding and is not suitable [46]. An estimate near $+2.0e$ also correlates with empirically assigned Si charges in earlier nonbonded models of $+2.1e$ (CLAYFF) [47] and $+2.4e$ (BKS) [48], of which only the BKS model is stable for silica and uses a more specialized Buckingham potential. We chose a Si charge at the higher end of $+2.4 \pm 0.2e$, which enhances the structural stability of SiO_2 in the simulation (Table 1). The nonbond diameter σ for Si of 1.80 Å was chosen to reproduce the Si-O bond length of 1.60 Å. This σ value for Si is less than half of σ for the bonded model due to the loss of electrons (higher positive charge of $+2.4e$), as well as due to the loss of bonded terms and of associated exclusion rules between bonded atoms [9]. The nonbond diameter σ for O remains approximately the same as in the bonded model [9]. The gain in negative charge (higher negative charge of $-1.2e$) causes expansion, which is approximately compensated by contraction due to the loss of bonded terms and of associated exclusion rules between bonded atoms. The combination of σ values and ϵ values represents the effective ratio of ionic radii of the Si cation to the O anion, and this ratio is essential to reproduce the corresponding crystal lattice [49]. The relatively high ϵ value for Si of 0.3 kcal/mol (1.26 kJ/mol) supports repulsion in the LJ potential to counterbalance strong electrostatic attraction (Table 1). A much smaller ϵ value for O supports deformations of the comparatively large nonbond diameter (σ) and a Si–O bond length of 1.60 Å. However, we caution that, while useful for the simulation of melts and glasses, the use of nonbonded silica parameters is a rather strong simplification.

Using these parameters (Table 1), the crystal structures of α -quartz [50] and α -cristobalite [51] from X-ray data are reproduced with relatively small deviations from the original positions and lattice parameters. The computed densities differ by 1.1% and 3.9% from experimental data, respectively. The ionic model can be subsequently applied to amorphous silica to capture changes in coordination, flow, and buildup of porous structures using nonbond-only forces. Silicon atoms at the top atomic layer of Mo_3Si were also partially oxidized ($+1.2e$) before full conversion to SiO_2 .

MoO_3 produced in the reaction (Fig. 1a) was represented by coarse-grain beads using the 12–6 LJ potential with parameters σ and ϵ (Table 1). We neglected the inclusion of all atoms as MoO_3 is relatively isotropic and has a small dipole moment. The interaction with silica was thus not significantly affected. The main function of gaseous MoO_3 was the creation of excluded volume in the silica morphology depending on the area density of Mo and Si on the surface and on the release rate. As details of the oxidation mechanism of Mo and Mo_3Si at the electronic structure level remain largely unknown, [4,6,52] using a simple model of MoO_3 (and similar to MoO_2) also involves less assumptions. The parameter σ represents the approximate size of MoO_3 in the vapor phase [33,53], and ϵ the approximate polarizability. The increase in volume from Mo to MoO_3 during the reaction creates outward pressure and exerts stress on the silica layer that affects the stability and morphology. The MoO_3 parameters were fine-tuned by test simulations at different temperatures to maintain adhesion of the silica layer throughout molecular dynamics simulations. This rationale can also be applied to other systems where porous oxides are shaped by evaporation of a gas.

2.8. Experimental data

Experimental data for comparison to the simulation results are reproduced from prior publications with the exception of the 3D reconstruction of an oxidized Mo_3Si sample from STEM images (Fig. 4g), which was obtained following the procedure in ref. [31].

3. Results and discussion

First, we analyzed the development of silica scale in the absence of volatile oxide evaporation. Then, we included MoO_3 evaporation in

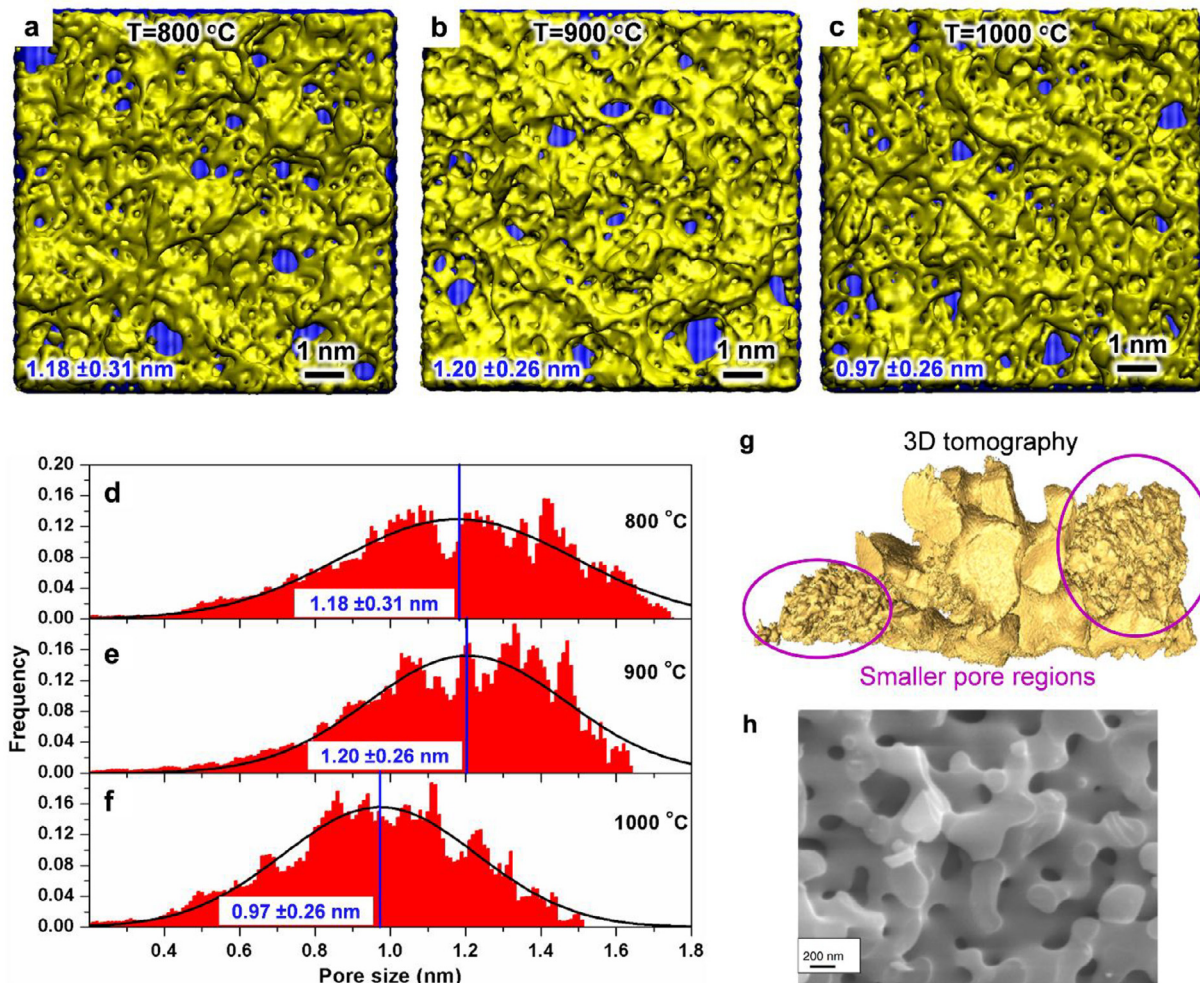


Fig. 4. The morphology of 3 nm thick silica layers on oxidized Mo₃Si surfaces from reactive molecular dynamics simulation and from experimental data including 3D electron tomography and SEM images. (a–c) Snapshots from the simulation at 800 °C, 900 °C, and 1000 °C with a 10 × 10 nm² area in top view. Evaporation of MoO₃ leads to the formation of pores and open channels. The average pore size decreases from 1.2 nm to 1.0 nm at higher temperature. The rate of layer-by-layer oxidation was 0.25 nm per cycle. (d–f) Temperature effect on average pore size and pore size distribution in the models at 800 °C, 900 °C, and 1000 °C. The pore analysis is based on a ray tracing algorithm using a spherical probe of 0.1 Å diameter (see methods). (g) 3D morphology of a fully oxidized Mo₃Si sample of approximately micrometer size obtained from a tilt series of STEM images (see ref. [31] for the protocol). Regions of widely variable pore sizes are seen. (h) Silica morphology upon oxidation of Mo₃Si for 10 min at 1100 °C in air obtained by SEM measurements (from ref. [11]). The micrometer-size sample and long time scale lead to very large and structured pores, beyond feasibility of current simulations. (For interpretation of the references to colour in this figure legend, the reader is referred to the web version of this article.)

the simulation and explain the difference in silica structure, the effect of temperature, and oxidation rate on the morphology in comparison with experimental measurements. The protocol of layer-by-layer reactive simulation of oxidation is promising to study oxidation reactions at a practical scale and can be applied to other chemistries.

3.1. Silica morphology in the absence of MoO₃ evaporation

In experiments, oxidation of pure Mo₃Si at 800 °C leads to the formation of a stable superficial silica layer as seen by in-situ TEM (Fig. 3a) [28]. After 24 min exposure to oxygen at 800 °C, the sample shows complete silica coverage on the Mo₃Si surface with a layer thickness of 1 to 2 nm, including nanometer-size pores. While different (h k l) crystallographic surfaces are oxidized at different rates, it is apparent that the silica layer is porous enough to allow oxygen penetration to the bulk. Grain re-orientation and movement was also observed.

In the simulation using a (10 nm)³ supercell of Mo₃Si, we obtained the structure of the porous silica glass in all-atomic detail (Fig. 3b). Here, we delete Mo atoms as the oxidation progresses to exclude the influence of volatile MoO₃ gas. The models show the emergence of local silica ring and chain structures that create the porous superficial

silica phase. The porosity originates from the 3:1 stoichiometry of Mo₃Si in which silicon is the minor component and, upon oxidation to SiO₂, silica cannot continuously (densely) cover the alloy surface (Fig. 3c). Accordingly, the silica tetrahedra assume a spatial arrangement with variable size distribution of clusters, rings, and chains. The inspection of the pore structure of a 3 nm thick silica layer shows irregularly shaped pores with sizes of less than 1 nm. The side view of the silica layer also shows nanometer-size channels that allow direct transport of oxygen molecules from the gas phase through the silica layer to the Mo₃Si surface (green highlight in Fig. 3c).

We further studied the effect model size on the results by increasing the dimensions to 100 × 100 × 100 nm³, corresponding to 64 million atoms (Figs. 3d–f). At this very large scale of all-atom simulations, the morphology looks comparable to the TEM images from experiments (Fig. 3a). The pore size distribution is very similar to the 10 nm-scale simulation, including local openings up to about 2 nm and continuous regions (Fig. 3d and e). The analysis of a much thicker silica layer of 10 nm depth formed on the alloy surface, in side view, shows that there are no remaining nanometer-sized channels that directly connect the gas phase and the Mo₃Si surface (Fig. 3f).

We conclude from the small and large simulations that the average pore size is less than 1 nm without MoO₃ evaporation. Further

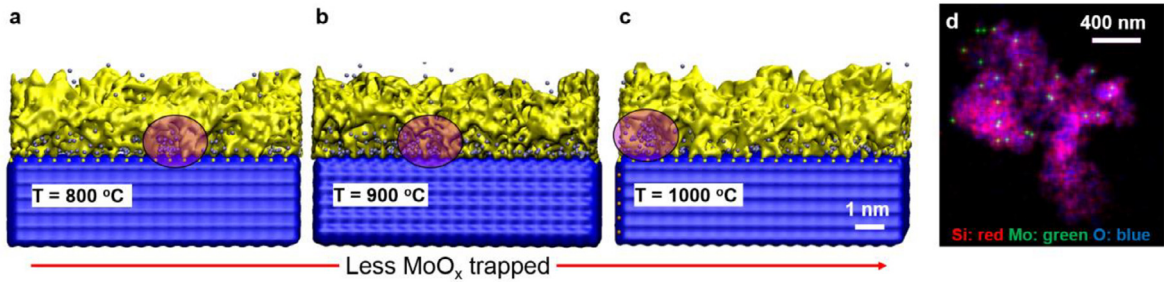


Fig. 5. Trapping of MoO₃ in the silica layer at the nanometer scale according to reactive molecular dynamics and measurements by EDS. (a–c) The morphology of 3 nm thick silica layers in side view at 800 °C, 900 °C, and 1000 °C shows different levels of MoO₃ inclusion (box length 10 nm). Some oxide molecules cannot exit due to the limited size of pores and channels. More MoO_x is trapped at lower temperature and less at higher temperature in the simulation. (d) EDS mapping shows trapping of Mo oxides in the silica sample produced after complete A15 oxidation (several 100³ nm³) (from ref. [31]).

tests at different temperatures (900 and 1000 °C) also showed no noteworthy differences in silica morphology. The violent evaporation of MoO₃, if present, would break open such small pores and establish channels in the superficial silica scale in the nascent stages as observed in experiment [28]. For near atomically thin silica layers up to 1 nm, the evaporation of Mo₃Si has only limited impact on the structure of the silica layer. For thicker layers formed upon continuous oxidation in experiment, it has been shown that, after a certain thickness in Mo–Si–B alloys, borosilicate has the potential to form a closed layer to offer strong oxidation protection [54].

3.2. Silica morphology as function of temperature and the role of MoO₃

Qualitative changes in the morphology of the silica film are seen upon inclusion of MoO₃ evaporation in the simulation of Mo₃Si oxidation (Fig. 4a–c). The silica scale (yellow) on the Mo₃Si surface (blue) shows larger pores as well as a larger number of direct nano-channels from the alloy surface through the 3 nm thick silica layer. The largest pore size is approximately 1.7 nm versus 1.1 nm in the absence of MoO₃ evaporation (Fig. 3b and c). The distribution of pore sizes is nevertheless broad (Fig. 4f). The average pore size decreases slightly at higher temperature from approximately 1.2 nm at 800 and 900 °C to 1.0 nm at 1000 °C (Fig. 4a–f). The occurrence of larger pores is diminished from 800 °C to 900 °C (Fig. 4d and e), and further shifts to smaller pores and narrower pore size distribution with a smaller standard deviation at 1000 °C (Fig. 4f). The smaller pore size and narrower distribution at higher temperature are related to a decrease in viscosity of silica and more rapid evaporation of MoO₃. At the same time, coarsening may act to increase the pore size, or contain the reduction in pore size.

The data from molecular dynamics simulation are in qualitative agreement with a reduction of pore size with increased temperature by mapping data from elemental dispersive spectroscopy (EDS) [31]. The experiments also show that long enough exposure times will entirely oxidize the A15 sample (Fig. 4g). 3D electron tomography of the resulting structures shows different regions in the sample that contain different pore size distributions, often on the order of 20–30 nm [31]. Overall, a large variation in pore size from few nanometers to nearly 100 nm is found and the resolution is about one nanometer (Fig. 4g). SEM images of oxidized Mo₃Si samples of several micrometer size have also shown more regular silica pores of large nanometer size (Fig. 4h) [11]. These pores can be mostly classified as mesopores (2–50 nm) and macropores (>50 nm), consistent with electron tomography results. Overall, silica scale formed upon oxidation of the A15 phase is porous and unlikely to form a fully protective oxide layer.

The simulations are a first step toward understanding the mechanism of oxidation at the atomic scale, at a resolution that remains difficult to reach by electron tomography and microscopy methods, and provide more detailed information about the dynamics. A major

limitation, however, is that the reaction rates in the simulation are about 10³ to 10⁶ times faster than in experiment. Therefore, the model systems initially develop small pores, similar as seen in experiments in the initial stages (Fig. 3a). The model systems subsequently oxidize more rapidly than in laboratory conditions, without enough time to grow and rearrange into larger pores from 0 to ~100 nm size, or larger near the oxide/gas interface [31].

The MoO₃ generated at the Mo₃Si–silica interface exerts forces on the silica and changes the morphology. The simulations show some trapped molybdenum oxide in the porous silica (Fig. 5a–c). Trapping of MoO_x is also observed by imaging of samples with EDS (Fig. 5d) [31]. The inclusion of MoO_x is higher at 800 °C and decreases toward 1000 °C in the simulation, which is the same trend as in measurements. The composition of trapped MoO_x, which is solid or a viscous liquid in this temperature range [12], maybe of variable stoichiometry with 2 < x < 3, and be trapped in the pores until eventual conversion to the MoO₃ and evaporation into the gas phase [13,31]. The model here does not further distinguish these details, assuming one coarse-grain bead per MoO₃ formula unit, and shows potential kinetic pathways in relation to the silica morphology. It is likely that for very long simulation times the trapped MoO₃ beads would eventually escape as a gas. Experiments have shown that for longer oxidation times all trapped metal oxide vaporizes [31].

3.3. Silica morphology for different rates of oxidation

The oxidation of Mo₃Si was studied as a function of different relative reaction rates by molecular dynamics simulation (Fig. 6). The relative rate of reaction, equivalent to oxygen partial pressure, was represented by the magnitude of Δz per reaction cycle. A thicker layer Δz oxidized per reaction cycle, i.e., per unit time, corresponds to higher oxygen partial pressure and a higher rate. The oxidation at a smaller rate between 0.1 nm and 0.25 nm per cycle leads to well-defined porous silica layers, evaporation of MoO₃, as well as detachment of small silica particles (Fig. 6a and b). Intermediate rates of oxidation of 0.25 nm per cycle increased the release of molybdenum oxide and changed the amount of detached silica clusters (Fig. 6c). Higher rates of oxidation of 0.5–1.0 nm per cycle, equal to the oxidation of multiple atomic layers per reaction cycle, exerted excessive pressure by the MoO₃ gas so that parts of or entire silica layers were broken off (Fig. 6d, e). For these different reaction rates, two forces oppose each other. Electrostatic interactions bind the superficial silica scale to the partially oxidized Si atoms at the alloy/oxide interface. On the other hand, the pressure of the evaporating MoO₃ beads destabilizes the silica layer. Therefore, different patterns of silica morphology and cohesion evolve, and silica pieces can break off if the mechanical force of gas evaporation exceeds the bonding forces within emergent silica clusters and the porous structure. In experiment, pulsed oxidation is often used to set a certain reaction rate. It can be difficult to measure the oxidation rate experimentally, however, and the

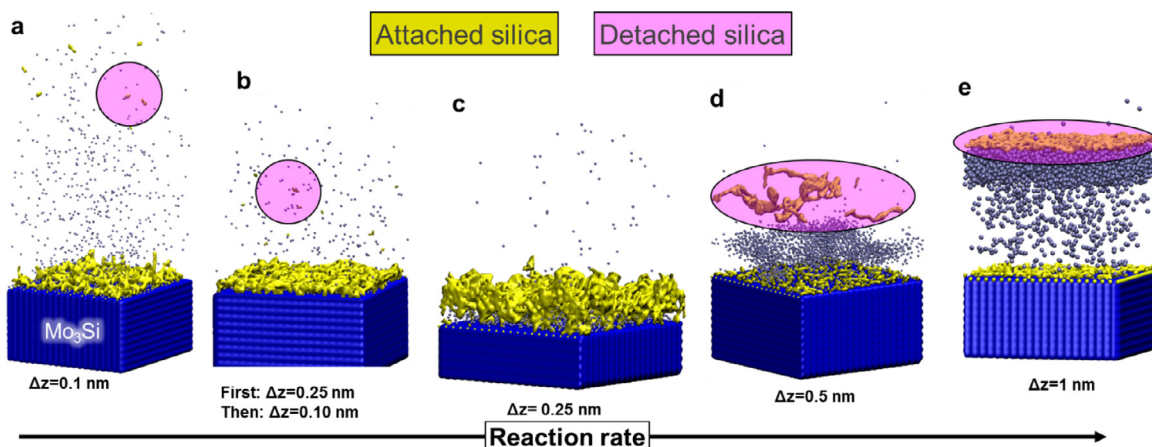


Fig. 6. Effect of oxidation rate on silica morphology at $T = 900\text{ }^{\circ}\text{C}$ according to molecular dynamics simulation (10 nm side length). The reaction rate is represented by a variation in sample thickness oxidized per reaction cycle Δz . (a) $\Delta z = 0.1\text{ nm}$ represents a low oxidation rate. (b) The oxidation rate was $\Delta z = 0.25\text{ nm}$ for the first 0.5 nm layer thickness and $\Delta z = 0.1\text{ nm}$ for subsequent layers. (c) $\Delta z = 0.25\text{ nm}$ represents an intermediate reaction rate. (d) $\Delta z = 0.5\text{ nm}$ and (e) $\Delta z = 1\text{ nm}$ represent a high oxidation rate, whereby the pressure of released MoO_3 gas ruptures the superficial silica layer. The exit of MoO_3 gas and, in some cases, small silica clusters can be seen.

simulations provide insight into the mechanics of the processes and possible outcomes for Mo_3Si oxidation.

The stability and pore size of the silica layer are further affected by the temperature and rate of MoO_3 generation. Thereby, growth of a stable silica layer also limits access of O_2 to the surface. Diffusion limitations can slow down the reaction rate and support the formation of large pores (Fig. 4h). In future work, the simulation protocol can be modified to account for oxygen accessibility and to explore the impacts of limited diffusion over longer time scales.

In addition, several aspects at the atomic and electronic scale are still unknown. O_2 molecules initially undergo physisorption and extensive adsorption-desorption cycles. This period continues for milliseconds to seconds [11] and meanwhile individual molecules develop covalent bonds with superficial Mo and Si atoms via electron transfer from the metal to O_2 molecules. Then, a series of intermediates containing bound molecular O_2 , atomic oxygen, M-O-M bridges, MO-O-(MO) and other motifs ($M = \text{metal}$) likely appears, accompanied by multi-stage electron transfer and an increase in oxidation state. Oxygen is available in excess and the reaction proceeds from the intermediates to the final products such as MoO_2 , MoO_3 , other MoO_x species, and SiO_2 . [14] Thereby, the oxidation reaction develops added heat and more rapidly oxidizes Mo to MoO_3 gas than Si to SiO_2 (pesteing), which can change the composition of the Mo_3Si alloy near the surface to Mo_5Si_3 and other Mo-Si ratios [4,11,15,31]. The elucidation of more specific details from quantum mechanical simulations and molecular dynamics simulations would be beneficial, although it is also challenging due to the multiscale and dynamic nature of the process. Our method utilizes confirmed knowledge from experiment and chemical theory to construct atomistic models of defined reactants and follows the reactions to defined end products. The approach essentially simulates pulse oxidation and does not require the inclusion of all transient species, thereby avoiding speculative assumptions. The layer-by-layer simulation protocol with appropriate force fields can guide in possible reaction paths and morphology development of the oxidized material as a function of the elemental composition, surface structure, and initial morphology.

4. Conclusions

We examined the oxidation of the Mo_3Si A15 alloy using reactive molecular dynamics simulations at 800 to 1000 $^{\circ}\text{C}$ in comparison to in-situ TEM, electron tomography, and EDS experiments. We introduced a new protocol for the reactive simulation of layer-by-layer oxidation cycles and used simple force field parameters for reactants,

products, and modeling the transition. In the absence of MoO_3 evaporation, a porous silica layer with small average pore sizes near 0.8 nanometers was formed. It corresponds to an “equilibrium” morphology and no open channels for gas evaporation were found at a thickness of the silica scale of 3 nm or more. Upon inclusion of MoO_3 evaporation, the morphology changed to porous silica layers with open channels and somewhat increased average pore size to 1.2 nm. Increased temperature leads to a reduction of the average pore size and a narrower pore size distribution, qualitatively consistent with experimental measurements. The porosity and stability of the silica layer is also determined by the rate, which was tested in a range from 0.1 to 1 nm layer thickness per reaction cycle. Very fast oxidation may exert a pressure that is sufficient to break down the cohesion of nascent silica nanostructures to the alloy surface. A moderate oxidation rate equal to or less than one atomic layer per cycle ($\sim 0.25\text{ nm}$) was found to be needed to form a stable silica layer. As a limitation in comparison to experimental data, the simulation times are orders of magnitude shorter. The simulations can thus only follow the early oxidation stages, and the pore structures of initial thin films is consistent with TEM data of nascent silica layers. Reactive simulations cannot currently describe the formation of larger pores up to 100 nm size after exposure for minutes. A key role for morphology development is played by the evaporation of MoO_x which is trapped in the nascent silica layer both in the simulation and according to EDS data.

The experimental data show a very wide distribution of pore sizes and shapes of oxidation products. Simulations and laboratory data indicate that the pore structure is large enough for oxygen penetration to the bulk, supporting continuous oxidation even at higher temperature. The reactive methods have been applied to millions of atoms, up to the large nanometer scale, and can be used for different (hkl) facets, grain boundaries, alloy compositions, temperatures, and reaction rates. The protocols and force fields, based on IFF, may also be applied to study the progression of oxidation reactions via islands rather than via entire atomic layers. The oxidation Mo-Si-B and other alloys is a complex process that benefits from further investigations including the refinement and validation of computational protocols at realistic length and time scales.

Declaration of Competing Interest

The authors declare that they have no known competing financial interests or personal relationships that could have appeared to influence the work reported in this paper.

Author Contributions

H. H. conceived the study and acquired funding. C. C. D. and H. H. developed the methods, curated the data, and carried out the analysis. J. Z. and J. M. curated experimental data and carried out the analysis. M. T. and J. H. P. carried out the analysis and validated the results. C. C. D., J. Z., J. M., M. T., J. H. P., and H. H. wrote the manuscript.

Acknowledgements

We acknowledge support from the Office of Naval Research (MURI N00014-14-1-0675) and the National Science Foundation (DMR 1623947). J.M. acknowledges the support by STROBE: A National Science Foundation Science & Technology Center (DMR 1548924). The allocation of computational resources at the CU Biofrontiers Computing Cluster and at the Ohio Supercomputing Center is acknowledged. This work further used resources of the Oak Ridge Leadership Computing Facility at the Oak Ridge National Laboratory, which is supported by the Office of Science of the U.S. Department of Energy under Contract No. DE-AC05-00OR22725, the Argonne Leadership Computing Facility, which is a DOE Office of Science User Facility supported under Contract DE-AC02-06CH11357, and the Janus supercomputer, which is supported by the National Science Foundation (award number CNS-0821794).

Supplementary materials

Supplementary material associated with this article can be found in the online version at doi:[10.1016/j.actamat.2020.01.048](https://doi.org/10.1016/j.actamat.2020.01.048).

References

- [1] G. Koch, J. Varney, N. Thompson, O. Moghissi, M. Gould, J. Payer, International Measures of Prevention, Application, and Economics of Corrosion Technologies Study, NACE International, Houston, TX, 2016.
- [2] J.H. Perepezko, The hotter the engine, the better, *Science* 326 (2009) 1068–1069.
- [3] W.O. Soboyejo, T.S. Srivatsan, *Advanced Structural Materials: Properties, Design Optimization, and Applications*, CRC Press, Boca Raton, 2006.
- [4] J.A. Lemberg, R.O. Ritchie, Mo–Si–B alloys for ultrahigh-temperature structural applications, *Adv. Mater.* 24 (2012) 3445–3480.
- [5] R. Sakidja, J.H. Perepezko, S. Kim, N. Sekido, Phase stability and structural defects in high-temperature Mo–Si–B alloys, *Acta Mater.* 56 (2008) 5223–5244.
- [6] T. Parthasarathy, M. Mendiratta, D. Dimiduk, Oxidation mechanisms in Mo-reinforced Mo₂SiB₂ (T2)–Mo₃Si alloys, *Acta Mater.* 50 (2002) 1857–1868.
- [7] H. Heinz, T.-J. Lin, R.K. Mishra, F.S. Emami, Thermodynamically consistent force fields for the assembly of inorganic, organic, and biological nanostructures: the interface force field, *Langmuir* 29 (2013) 1754–1765.
- [8] J. Liu, E. Tennesen, J. Miao, Y. Huang, J.M. Rondinelli, H. Heinz, Understanding chemical bonding in alloys and the representation in atomistic simulations, *J. Phys. Chem. C* 122 (2018) 14996–15009.
- [9] F.S. Emami, V. Puddu, R.J. Berry, V. Varshney, S.V. Patwardhan, C.C. Perry, H. Heinz, Force field and a surface model database for silica to simulate interfacial properties in atomic resolution, *Chem. Mater.* 26 (2014) 2647–2658.
- [10] H. Heinz, R.A. Vaia, B.L. Farmer, R.R. Naik, Accurate simulation of surfaces and interfaces of face-centered cubic metals using 12–6 and 9–6 Lennard-Jones potentials, *J. Phys. Chem. C* 112 (2008) 17281–17290.
- [11] F. Rioult, S. Imhoff, R. Sakidja, J. Perepezko, Transient oxidation of Mo–Si–B alloys: effect of the microstructure size scale, *Acta Mater.* 57 (2009) 4600–4613.
- [12] D.R. Lide, *CRC Handbook of Chemistry and Physics*, 96th ed., CRC Press, Boca Raton, FL, 2015.
- [13] N. Floquet, O. Bertrand, J.J. Heizmann, Structural and morphological studies of the growth of MoO₃ scales during high-temperature oxidation of molybdenum, *Oxid. Metals* 37 (1992) 253–280.
- [14] S. Zhang, D. Zhao, *Aerospace Materials Handbook*, CRC Press, Boca Raton, 2016.
- [15] D.M. Dimiduk, J.H. Perepezko, Mo–Si–B alloys: developing a revolutionary turbine-engine material, *MRS Bull.* 28 (2003) 639–645.
- [16] M. Mendiratta, T. Parthasarathy, D. Dimiduk, Oxidation behavior of α Mo–Mo₃Si–Mo₂SiB₂ (T2) three phase system, *Intermetallics* 10 (2002) 225–232.
- [17] D. Helmick, G. Meier, F. Pettit, The development of protective borosilicate layers on a Mo-3Si-1B (weight percent) alloy, *Metallurg. Mater. Trans. A* 36 (2005) 3371–3383.
- [18] S. Ochiai, Influence of the addition of Cr and Al elements to the Mo₃Si intermetallic alloy on the phase construction and the oxidation behavior, *Materials Science Forum*, Trans Tech Publications, Switzerland (2003) 1771–1776.
- [19] I. Rosales, H. Martinez, D. Bahena, J.A. Ruiz, R. Guardian, J. Colin, Oxidation performance of Mo₃Si with Al additions, *Corrosion Sci.* 51 (2009) 534–538.
- [20] C.C. Dharmawardhana, R. Sakidja, S. Aryal, W.Y. Ching, Temperature dependent mechanical properties of Mo–Si–B compounds via Ab-initio molecular dynamics, *APL Mater.* 1 (2013) 012106.
- [21] C. Dharmawardhana, R. Sakidja, S. Aryal, W. Ching, In search of zero thermal expansion anisotropy in Mo₅Si₃ by strategic alloying, *J. Alloys Compounds* 620 (2015) 427–433.
- [22] N.E. Singh-Miller, N. Marzari, Surface energies, work functions, and surface relaxations of low-index metallic surfaces from first principles, *Phys. Rev. B* 80 (2009) 235407.
- [23] M. Nathanson, K. Kanhaiya, A. Pryor, J. Miao, H. Heinz, Atomic-Scale structure and stress release mechanism in core–shell nanoparticles, *ACS Nano* 12 (2018) 12296–12304.
- [24] H. Ramezani-Dakheel, P.A. Mirau, R.R. Naik, M.R. Knecht, H. Heinz, Stability, surface features, and atom leaching of palladium nanoparticles: toward prediction of catalytic functionality, *Phys. Chem. Chem. Phys.* 15 (2013) 5488–5492.
- [25] J. Zhou, Y. Yang, Y. Yang, D.S. Kim, A. Yuan, X. Tian, C. Ophus, F. Sun, A.K. Schmid, M. Nathanson, H. Heinz, Q. An, H. Zeng, P. Ercius, J. Miao, Observing crystal nucleation in four dimensions using atomic electron tomography, *Nature* 570 (2019) 500–503.
- [26] B. Briggs, N.M. Bedford, S. Seifert, H. Koerner, H. Ramezani-Dakheel, H. Heinz, R.R. Naik, A. Frenkel, M.R. Knecht, Atomic-Scale identification of Pd leaching in nanoparticle catalyzed CC coupling: effects of particle surface disorder, *Chem. Sci.* 6 (2015) 6413–6419.
- [27] I.L. Geada, H. Ramezani-Dakheel, T. Jamil, M. Sulpizi, H. Heinz, Insight into induced charges at metal surfaces and bionterfaces using a polarizable Lennard-Jones potential, *Nat. Comm.* 9 (2018) 716.
- [28] A. Gulec, X.-x. Yu, M. Taylor, A. Yoon, J.-M. Zuo, J. Perepezko, L. Marks, Early stage of oxidation of Mo₃Si by in-situ environmental TEM, *Corrosion* 74 (2018) 361–374.
- [29] R. Xu, C.-C. Chen, L. Wu, M.C. Scott, W. Theis, C. Ophus, M. Bartels, Y. Yang, H. Ramezani-Dakheel, M.R. Sawaya, H. Heinz, L.D. Marks, P. Ercius, J. Miao, Three-Dimensional coordinates of individual atoms in materials revealed by electron tomography, *Nat. Mater.* 14 (2015) 1099–1103.
- [30] J. Miao, P. Ercius, S.J.L. Billinge, Atomic electron tomography: 3D structures without crystals, *Science* 353 (2016) 1380.
- [31] J.H. Zhou, M. Taylor, G.A. Melinte, A.J. Shahani, C.C. Dharmawardhana, H. Heinz, P.W. Voorhees, J.H. Perepezko, K. Bustillo, P. Ercius, J.W. Miao, Quantitative characterization of high temperature oxidation using electron tomography and energy-dispersive X-ray spectroscopy, *Sci. Rep.* 8 (2018) 10239.
- [32] D. Templeton, C.H. Dauben, The crystal structure of Mo₃Si, *Acta Cryst.* 3 (1950) 261–262.
- [33] E.F. Fialko, A.V. Kikhtenko, V.B. Goncharov, K.I. Zamaraev, Molybdenum oxide cluster ions in the gas phase: structure and reactivity with small molecules, *J. Phys. Chem. A* 101 (1997) 8607–8613.
- [34] W.R. Tyson, W.A. Miller, Surface free-energies of solid metals – Estimation from liquid surface-tension measurements, *Surf. Sci.* 62 (1977) 267–276.
- [35] H. Choe, D. Chen, J.H. Schneibel, R.O. Ritchie, Ambient to high temperature fracture toughness and fatigue-crack propagation behavior in a Mo-12Si-8.5B (at.%) intermetallic, *Intermetallics* 9 (2001) 319–329.
- [36] H.L. Zhao, M.J. Kramer, M. Akinc, Thermal expansion behavior of intermetallic compounds in the Mo–Si–B system, *Intermetallics* 12 (2004) 493–498.
- [37] K.K. Unger, *Porous Silica*, 16, Elsevier, Amsterdam, 1979.
- [38] T.F. Willems, C.H. Rycroft, M. Kazi, J.C. Meza, M. Haranczyk, Algorithms and tools for high-throughput geometry-based analysis of crystalline porous materials, *Micropor. Mesopor. Mater.*, 149, 2012, pp. 134–141.
- [39] E. Haldoupis, S. Nair, D.S. Sholl, Efficient calculation of diffusion limitations in metal organic framework materials: a tool for identifying materials for kinetic separations, *J. Am. Chem. Soc.* 132 (2010) 7528–7539.
- [40] M. Treacy, M. Foster, Packing sticky hard spheres into rigid zeolite frameworks, *Micropor. Mesopor. Mater.* 118 (2009) 106–114.
- [41] M. Haranczyk, *Zeo++ program*, <http://zeoplusplus.org/>.
- [42] A.J. Jones, C. Ostrouchov, M. Haranczyk, E. Iglesia, From rays to structures: representation and selection of void structures in zeolites using stochastic methods, *Micropor. Mesopor. Mater.* 181 (2013) 208–216.
- [43] H. Heinz, H. Koerner, K.L. Anderson, R.A. Vaia, B.L. Farmer, Force field for mica-type silicates and dynamics of octadecylammonium chains grafted to montmorillonite, *Chem. Mater.* 17 (2005) 5658–5669.
- [44] C.C. Dharmawardhana, K. Kanhaiya, T.-J. Lin, A. Garley, M.R. Knecht, J. Zhou, J. Miao, H. Heinz, Reliable computational design of biological-inorganic materials to the large nanometer scale using interface-FF, *Mol. Sim.* 43 (2017) 1394–1405.
- [45] A. Pedone, Properties calculations of silica-based glasses by atomistic simulations techniques: a review, *J. Phys. Chem. C* 113 (2009) 20773–20784.
- [46] H. Heinz, U.W. Suter, Atomic charges for classical simulations of polar systems, *J. Phys. Chem. B* 108 (2004) 18341–18352.
- [47] R.T. Cygan, J.-J. Liang, A.G. Kalinichev, Molecular models of hydroxide, oxyhydroxide, and clay phases and the development of a general force field, *J. Phys. Chem. B* 108 (2004) 1255–1266.
- [48] B.W.H. van Beest, G.J. Kramer, R.A. van Santen, Force fields for silicas and aluminophosphates based on Ab initio calculations, *Phys. Rev. Lett.* 64 (1990) 1955–1958.

- [49] J.E. Huheey, E.A. Keiter, R.L. Keiter, *Inorganic Chemistry - Principles of Structure and Reactivity*, 4th ed., Harper Collins College Publishers, New York, 1993.
- [50] K. Kihara, An X-ray study of the temperature-dependence of the quartz structure, *J. Mineral.* 2 (1990) 63–77.
- [51] P. Dera, J.D. Lazarz, V.B. Prakapenka, M. Barkley, R.T. Downs, New insights into the high-pressure polymorphism of SiO₂ cristobalite, *Phys. Chem. Miner.* 38 (2011) 517–529.
- [52] E.A. Gulbransen, K.F. Andrew, F.A. Brassart, Oxidation of molybdenum 550-Degrees-C to 1700-Degrees-C, *J. Electrochem. Soc.* 110 (1963) 952–959.
- [53] T. Charlu, O. Kleppa, A calorimetric determination of the enthalpy of vaporization of MoO₃, *J. Chem. Thermodyn.* 3 (1971) 697–700.
- [54] J.S. Park, R. Sakidja, J.H. Perepezko, Coating designs for oxidation control of Mo–Si–B alloys, *Scripta Mater.* 46 (2002) 765–770.